Quantum wave packet study of nonadiabatic effects in O(Â¹D) + Hâ â OH + H

ARTICLE *in* THE JOURNAL OF PHYSICAL CHEMISTRY A · NOVEMBER 1999

Impact Factor: 2.69 · DOI: 10.1021/jp991601j

4 AUTHORS, INCLUDING:

Stephen K. Gray
Argonne National Laboratory
262 PUBLICATIONS **8,670** CITATIONS

Carlo Petrongolo
Università degli Studi di Siena
67 PUBLICATIONS **1,315** CITATIONS

Karen Drukker
University of Chicago
87 PUBLICATIONS **1,059** CITATIONS

Quantum Wave Packet Study of Nonadiabatic Effects in O(¹D) + H₂ → OH + H

Stephen K. Gray*

Chemistry Division, Argonne National Laboratory, Argonne, Illinois 60439

Carlo Petrongolo

Department of Chemistry, University of Siena, Via Aldo Moro, I-53100 Siena, Italy

Karen Drukker and George C. Schatz

Chemistry Department, Northwestern University, 2145 Sheridan Road, Evanston, Illinois 60208-3113

Received: May 17, 1999; In Final Form: July 27, 1999

We develop a wave packet approach to treating the electronically nonadiabatic reaction dynamics of O(¹D) + H₂ → OH + H, allowing for the $1^1A'$ and $2^1A'$ potential energy surfaces and couplings, as well as the three internal nuclear coordinates. Two different systems of coupled potential energy surfaces are considered, a semiempirical diatomics-in-molecules (DIM) system due to Kuntz, Niefer, and Sloan, and a recently developed ab initio system due to Dobbyn and Knowles (DK). Nonadiabatic quantum results, with total angular momentum $J = 0$, are obtained and discussed. Several single surface calculations are carried out for comparison with the nonadiabatic results. Comparisons with trajectory surface hopping (TSH) calculations, and with approximate quantum calculations, are also included. The electrostatic coupling produces strong interactions between the $1^1A'$ and $2^1A'$ states at short range (where these states have a conical intersection) and weak but, interestingly, nonnegligible interactions between these states at longer range. Our wave packet results show that if the initial state is chosen to be effectively the 1A′ state (for which insertion to form products occurs on the adiabatic surface), then there is very little difference between the adiabatic and coupled surface results. In either case the reaction probability is a relatively flat function of energy, except for resonant oscillations. However, the 2A′ reaction, dynamics (which involves a collinear transition state) is strongly perturbed by nonadiabatic effects in two distinct ways. At energies above the transition state barrier, the diabatic limit is dominant, and the 2A′ reaction probability is similar to that for 1A″, which has no coupling with the other surfaces. At energies below the barrier, we find a significant component of the reaction probability from long range electronic coupling that effectively allows the wave packet to avoid having to tunnel through the barrier. This effect, which is observed on both the DIM and DK surfaces, is estimated to cause a 10% contribution to the room temperature rate constant from nonadiabatic effects. Similar results are obtained from the TSH and approximate quantum calculations.

I. Introduction

The reaction

$$O(^1D) + H_2(X^1\Sigma_g^+) \rightarrow OH(X^2\Pi) + H(^2S) \qquad (1)$$

has long served as the prototypical insertion reaction. It is exoergic by almost 2 eV, and the lowest adiabatic potential surface ($1^1A'$) that correlates to both reactants and products includes a deep well associated with the ground electronic state of H₂O. (The zero-point energy of H₂O is ≈5 eV below the zero-point energy of the products.) Both products are easily detected, so there have been numerous experimental studies of thermal rate coefficients,[1,2] isotope effects,[3–6] product vibrational distributions,[7] rotational distributions,[8,9] integral cross sections,[10] and angular and translational distributions.[11–16] There have also been several theoretical studies of the ground singlet state potential surface[17–21] and its reaction dynamics.[22–28]

Recently there has been increasing interest in the reaction dynamics associated with excited states that also correlate to O(¹D) + H₂.[29–35] Figure 1 shows a schematic diagram of the key electronic states for collinear and nearly collinear OHH geometries. The bottom panel considers collinear OHH geometries. Actually, O(¹D) splits into a Σ, a doubly degenerate Π, and a doubly degenerate Δ component, so that the reactants in reaction 1 correlate with five electronic states. The Δ state is purely repulsive, and can only play a role in the reaction dynamics through its Coriolis interactions with the other states, which turns out not to be very important.[35] This state is not depicted. The Σ surface is the lowest energy surface while the reagents approach, with a very small barrier (< 0.5 kcal/mol or 0.02 eV), but it correlates to the excited A²Σ state of the OH product, and thus it cannot contribute to reaction. Only the Π state connects the reagent and product states, but there is a barrier to reaction of around 2 kcal/mol (0.09eV). The top part shows how this picture changes for bent geometries. Here we show only the 1A′ and 2A′ components that come from the Σ and Π states. (For simplicity, we often omit the singlet spin labels on the various electronic states.) These have a conical intersection at the position of the Σ/Π crossing, making it possible for reaction to occur out of either state. Not shown in this panel is the 1A″ state, which is the other component the Π

Nonadiabatic Effects in O(^{1}D) + H$_2$ → OH + H

J. Phys. Chem. A, Vol. 103, No. 47, 1999 **9449**
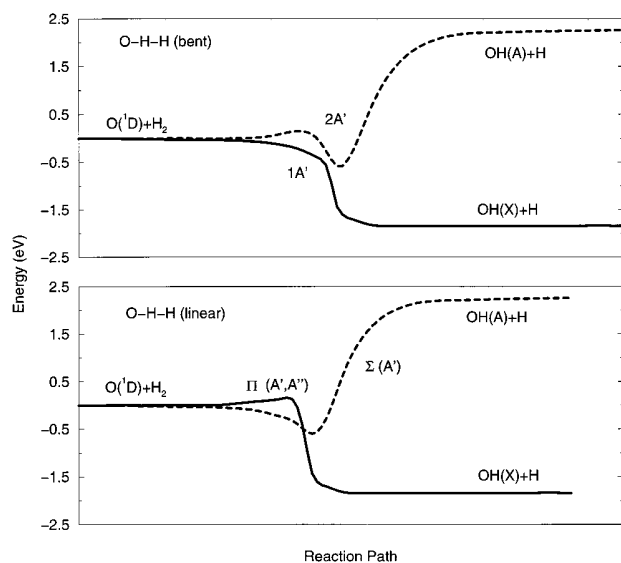
Figure 1. Schematic diagram of the two relevant electronic states for O(^{1}D) + H$_2$. As the reactants approach each other the initially degenerate surfaces split in energy. OH(X)+H corresponds to products. Top part: Surfaces for bent OHH geometries. Bottom part: Surfaces for collinear OHH geometries.

state in the bottom panel. This has the same collinear barrier as 2A′, but a lower bending frequency at the saddle point, so one expects that the reaction probability from this state will be larger than that from the 2A′ state. Note, however, that the 2A′ reaction probability would be zero if the dynamics were purely adiabatic, while the 1A″ state is not coupled to the other states, and is reactive in the adiabatic limit.

Although the behavior of the potential surfaces in Figure 1 is now well established, the role of the excited states in the reaction dynamics of reaction 1 is still the subject of considerable confusion. Interest in excited state effects has arisen recently as a result of several experiments[10,12,14−16] which show effects that are not consistent with a simple insertion reaction. In particular Che and Liu[12] measured differential cross sections for the O(^{1}D) + HD at a collision energy of 4.55 kcal/mol (0.197 eV) and found substantial deviation from the forward−backward symmetry found for theoretical studies based on the ground state surface.[21] In addition, similar measurements by other groups[15,16] on O(^{1}D) + H$_2$, HD and D$_2$ at energies as low as 1 kcal/mol (0.04 eV) indicate asymmetry in the differential cross sections. In other studies[14] the integral cross section was found to decrease with increasing energy for collision energies below 2 kcal/mol, as expected for an insertion reaction with no barrier, and to increase at higher energies, as expected for an abstraction reaction. This influences the O(^{1}D) + H$_2$ rate coefficients,[4] and it is observed that the high temperature rate coefficient is substantially higher than at room temperature. This activated behavior is not expected for reaction on the ground state surface.

These experimental studies have stimulated theoretical studies of O(^{1}D) + H$_2$ that include excited states. In one of these studies, the excited states were included only as uncoupled adiabatic states in quasi-classical trajectory (QCT) calculations.[33] Other studies[29−31,34] used trajectory surface hopping (TSH) methods[36,37] and involved two coupled states (1A′ and 2A′). The TSH studies included coupling due to electrostatic interactions that are important at short range (because of the conical intersection), but electronic Coriolis effects and long range electrostatic coupling were neglected. The conclusion of these studies is that the lowest state can account for most of the cross section at low collision energies ≤ 2 kcal/mol. The 2A′ and

1A″ states become important at high energy once the barrier to reaction on these states is surmounted. This produces the increase in the cross section with energy observed above 2 kcal/mol.

Important discrepancies between theory and experiment remain that are unresolved at this point. In particular, several groups have noted[38−40] that the agreement between the observed angular and translational energy distributions and those from TSH or adiabatic QCT calculations is worse when the excited states are included than when they are omitted. Also, Lee and Liu[41] have recently demonstrated that the 1A″ contribution to the cross section is larger for H$_2$ initial rotation state $j = 1$ compared to $j = 0$, the opposite of what was suggested by classical trajectory calculations.[33] In addition, the validity of the TSH method has been questioned in recent studies of other gas phase reactions,[42,43] so these criticisms might also be valid for O(^{1}D) + H$_2$.

In this paper, we present a new study of nonadiabatic effects in O(^{1}D) + H$_2$, based on three dimensional (total angular momentum J = 0) wave packet calculations. These calculations are based on similar technology to what was used in recent wave packet calculations for the ground state surface,[27,28] but in the present calculations we include for the coupled dynamics involving 1A′ and 2A′. We also present adiabatic results for the 1A″ surface, so that the relative reactivity of 2A′ and 1A″ can be determined. Electronic Coriolis coupling effects will not be included; however, a recent quantum study has shown[35] that they play a relatively minor role in the overall reactivity for this system.

Our calculations consider two sets of coupled potential surfaces, one being the semiempirical diatomics-in-molecules (DIM) surfaces that were developed by Kuntz, Niefer, and Sloan[30,31] and the other being the recently developed ab initio surfaces from Dobbyn and Knowles (DK).[44,45] Included in our analysis are comparisons with the results of other methods for describing the reaction dynamics, including the TSH method noted above, and the recent vibrationally adiabatic quantum scattering method of Drukker and Schatz.[35] We also make estimates of the effect of nonadiabacity on the thermal rate constant.

All of our quantum and our best TSH calculations are based on a diabatic representation where the electronic Hamiltonian is written as a 2 × 2 matrix that contains Σ-like and Π(A′)-like potentials along the diagonal, and an interaction potential $H_{\Sigma,\Pi}$ that vanishes for linear geometries. We use the terms "Σ diabat" and "Π-diabat" to refer to these states (even for nonlinear geometries), and "1A″" and "2A″" to refer to the adiabats that are obtained by diagonalizing the 2 × 2 matrix. In Drukker and Schatz,[35] another diabatic representation was introduced in which the A′ and A″ components of the Π state are rewritten in terms of complex exponentials so that they are also eigenfunctions of the electronic orbital angular momentum projection operator along the molecular axis. This alternative diabatic representation, in which the electronic Hamiltonian is 3 × 3 (or 5 × 5 if Δ states are included), is convenient for describing the Coriolis interactions. However if this interaction is left out, as in the present calculations, then the A′ and A″ states are not coupled, and it is easier to use the 2 × 2 diabatic representation in terms of Σ and Π(A′) states.

This paper is organized as follows. In section II we describe the diabatic model, potential surfaces, and briefly outline essential aspects of the wave packet and other dynamical methods employed by us. Section III presents the application to O(^{1}D) + H$_2$. Section IV summarizes our conclusions.

II. Model and Methods

A. Diabatic Hamiltonian Model. Here we present the two-state electronic Hamiltonian used in the present calculations. A more rigorous five-state description of the $O(^1D) + H_2$ reaction dynamics is presented by Drukker and Schatz.[35] Reactant Jacobi coordinates R, r, and $\cos\gamma$ are employed, with R being the O to center of H_2 distance, r being the H_2 distance, and $\cos\gamma$ the cosine of the angle between the vectors associated with R and r.

In the two-state approximation, electronic orbital angular momentum is neglected, so that the Hamiltonian operator H is given by an expression that is very similar to the single surface result. This Hamiltonian is

$$H = \frac{P^2}{2\mu} + \frac{\mathbf{l}^2}{2\mu R^2} + \frac{p^2}{2m} + \frac{\mathbf{j}^2}{2mr^2} + H^{el} \tag{2}$$

where $\mu = 2m_H m_O/(2m_H + m_O)$, $m = m_H/2$, P and p are radial momentum operators associated with R and r, respectively, $\mathbf{l}^2/2\mu R^2$ is the centrifugal term, $\mathbf{j}^2/2mr^2$ is the rotational energy term, which involves derivatives associated with $\cos\gamma$, and H^{el} is the electronic Hamiltonian. Since electronic angular momentum is not included, the total angular momentum $\mathbf{J}$ is given by $\mathbf{J} = \mathbf{j} + \mathbf{l}$, and the centrifugal term $\mathbf{l}^2/2\mu R^2$ gives rise to (nuclear) Coriolis coupling effects when the wave function is expressed in body-fixed coordinates. In this work, only $J = 0$ will be considered in the wave packet calculations ($\mathbf{l}^2 = \mathbf{j}^2$), and ∡-shifting[28] or J-shifting[46] approximations are used in performing the partial wave sums to determine cross sections and rate constants.

The wave function (or wave packet) is expanded in terms of diabatic electronic states, which we call $|\Sigma\rangle$ and $|\Pi\rangle$. (For brevity we use $|\Pi\rangle$ to denote the state associated with the A′ component, $\Pi(A')$, of the Π state.) These states depend not only on the electronic degrees of freedom, but on the nuclear degrees of freedom R, r, and $\cos\gamma$. However, it is assumed that these diabatic states have been suitably determined so that nuclear derivative terms associated with them, arising from the kinetic energy operators in eq 2, can be neglected. This, of course, is a key simplifying feature of a good diabatic representation since coupling matrix elements related to derivatives of the electronic states with respect to nuclear coordinates, which can be difficult to calculate (and sometimes divergent), do not occur. The Schrödinger equation then takes the form of a 2 × 2 matrix equation, with the nuclear kinetic energy terms in the Hamiltonian appearing along the diagonal, and the electronic Hamiltonian H^{el} appearing as a 2 × 2 matrix,

$$H^{el} = \begin{pmatrix} H_{\Sigma,\Sigma} & H_{\Sigma,\Pi} \\ H_{\Pi,\Sigma} & H_{\Pi,\Pi} \end{pmatrix} \tag{3}$$

where $H_{\Sigma,\Sigma}$ is the Σ diabat, $H_{\Pi,\Pi}$ is the $\Pi(A')$ diabat, and $H_{\Sigma,\Pi} = H_{\Pi,\Sigma}$ is the diabatic coupling potential. Note that the diabatic electronic matrix elements in the present treatment are real-valued functions, and are formally consistent with the use of real-valued electronic functions (e.g. cosines). This differs from the use of a complex exponential basis by Schatz and Drukker,[35] but is of course also a valid and equivalent representation. (See also the Introduction.)

Of course, all the matrix elements in eq 3 depend on the nuclear degrees of freedom, R, r, and $\cos\gamma$. If H^{el} is diagonalized, then the eigenvalues are the adiabatic potentials (1A′ and 2A′), and the derivatives of the eigenvectors with
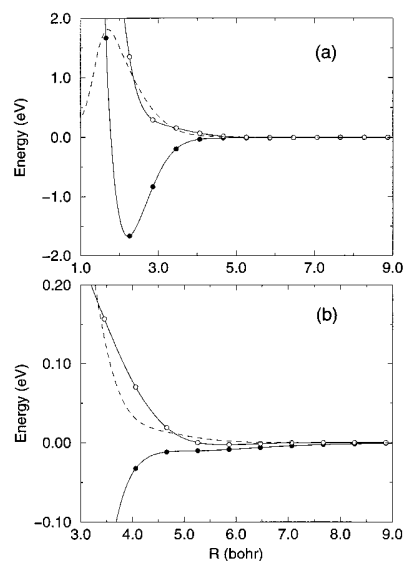
Figure 2. The DK diagonal diabatic energies, $H_{\Sigma,\Sigma}$ (solid curve with filled circles), $H_{\Pi,\Pi}$ (solid curve with open circles), and coupling $H_{\Sigma,\Pi}$ (dashed curve), averaged over an asymptotic H_2 ground vibration−rotation state. (a) presents a broad view of these matrix elements and (b) is a blowup of the longer range portion.

respect to the nuclear variables define the usual nonadiabatic coupling matrix elements that couple the adiabatic states.

B. Potential Energy Surfaces. The Dobbyn-Knowles (DK) potential surface[44,45] is based on high quality internally contracted multireference configuration interaction calculations. Although adiabatic states are produced in these calculations, a diabatization transformation was performed, so that the matrix elements $H_{\Sigma,\Sigma}$ $H_{\Pi,\Pi}$, and $H_{\Sigma,\Pi}$ were directly provided. This diabatization is based on calculating matrix elements associated with the component of the electronic orbital angular momentum operator and, in effect, constructing linear superpositions of the adiabatic states (i.e. diabatic states) that have significant Σ or Π character with respect to certain axes. The original theory of this approach was described by Rebentrost and Lester,[47] and a recent description that is more relevant to the present applications is given in Dobbyn et al.[48] Figure 2 illustrates the relevant diabatic energies and coupling for the DK surface. The $H_{\alpha,\alpha'}$ displayed in Figure 2 have been averaged over r and $\cos\gamma$, with weighting determined by the absolute square of an asymptotic H_2 ground vibration−rotation state. The top part, Figure 2a, gives a broad picture over a wide range of R values, whereas the lower part, Figure 2b, focuses on the diabats and coupling at longer range.

The DIM potential of Kuntz, Niefer, and Sloan[30,31] has been developed in a slightly different way than the DK surface. This potential is available in the adiabatic representation, and it is not straightforward to transform it to a diabatic representation using the procedure just described. Another procedure is possible, however, because in addition to the 1A′ and 2A′ surfaces we also have the 1A″ surface from the same DIM calculations.[34] This surface is similar to the Π diabat, $H_{\Pi,\Pi}$, so if we simply assume these are the same, it is possible to derive expressions for $H_{\Sigma,\Sigma}$ and $H_{\Sigma,\Pi}$ by inverting the following formulas, obtained from diagonalizing eq 3:

$$E(1A') = \frac{1}{2}[(H_{\Sigma,\Sigma} + H_{\Pi,\Pi}) - ((H_{\Sigma,\Sigma} - H_{\Pi,\Pi})^2 - 4H_{\Sigma,\Pi}^2)^{1/2}]$$

$$E(2A') = \frac{1}{2}[(H_{\Sigma,\Sigma} + H_{\Pi,\Pi}) + ((H_{\Sigma,\Sigma} - H_{\Pi,\Pi})^2 - 4H_{\Sigma,\Pi}^2)^{1/2}] \tag{4}$$

Nonadiabatic Effects in O(^{1}D) + H$_2$ → OH + H

J. Phys. Chem. A, Vol. 103, No. 47, 1999 **9451**

We used the DIM diabats defined this way in all of our calculations.

The DK and DIM potential surfaces are qualitatively similar, but there are some important quantitative differences. Perhaps the most noticeable difference is in the (collinear) barrier height for reaction on the 1A″ surface. This barrier is 2.3 kcal/mol on the DK surface and is located at r_{OH} = 3.09 a_0, r_{HH} = 1.46 a_0, with vibrational frequencies 3646, 271, and 661i cm^{-1}. On the DIM surface, the barrier is 3.7 kcal/mol, and is located at r_{OH} = 3.17 a_0, r_{HH} = 1.43 a_0, with frequencies of 4122, 174, 566i cm^{-1}. Another difference is in the long range part of the 1A′ potential, which is more attractive on the DIM than on DK surface. These differences make the 1A′ cross sections larger for the DIM surface, but the 1A″ and 2A′ cross sections (usually) larger on the DK surface.

C. Wave Packet Dynamics. The quantum dynamics calculations were carried out in a fashion similar to previous calculations for the 1A′ adiabatic dynamics.[27,28] The main difference, of course, is that the wave packet now also includes components associated with the two diabatic electronic states α = Σ and Π. The addition of the electronic degrees of freedom poses no difficulties with the J = 0 Hamiltonian being essentially the same as in refs 27 and 28 except that the adiabatic potential $V(R, r, \cos \gamma)$ is replaced by the 2 × 2 diabatic matrix, eq 3. We therefore only describe a few pertinent details.

The propagation scheme employed (see below) focuses on just the real part of the wave packet, which in terms of reactant Jacobi coordinates may be written

$$q^k(R, r, \cos \gamma) = \sum_\alpha \sum_j C^k_{j,\alpha}(R, r)\bar{P}_j(\cos \gamma)|\alpha\rangle \qquad (5)$$

where $\bar{P}_j$ are normalized Legendre polynomials, and $|\alpha\rangle$ formally represent the electronic states α = Σ and Π. The superscript k is used to denote iteration number or discrete time step. Evenly spaced grids are employed for R and r: with $x = R$ or r, $x_i = x_{min} + n\Delta x$, $n = 1,2,...,N_x$, $\Delta x = (x_{max} - x_{min})/(N_x + 1)$. The introduction of finite sized grids, as well as a finite rotational basis in j, effectively implies q^k is approximated by a large vector $\mathbf{q}^k$ and the Hamiltonian operator becomes a matrix $\mathbf{H}$.

The real wave packet propagation scheme[49] was employed, which features propagating the real vector $\mathbf{q}^k$ according to Mandelshtam and Taylor's damped Chebyshev iterations.[50,51] Introducing a linearly scaled Hamiltonian matrix $\mathbf{H}_s = a_s\mathbf{H} + b_s$, such that the eigenvalues of $\mathbf{H}_s$ lie within (−1,1), the damped Chebyshev iteration is

$$\mathbf{q}^{k+1} = \mathbf{A} \cdot (-\mathbf{A} \cdot \mathbf{q}^{k-1} + 2\mathbf{H}_s \cdot \mathbf{q}^k) \qquad (6)$$

here $\mathbf{A}$ is some appropriate matrix which damps the wave packet amplitude as it approaches the R and r grid edges. We take $\mathbf{A}$ to be a diagonal matrix with elements $a_R(R_i)a_r(r_j)$, where $a_x(x_i) = \exp[-c_x(x_i - x_a)^2]$ for $x_i \geq x_a$. In the real wave packet approach, the Chebyshev iterations above are identified with the real part of the *exact* Schrödinger time evolution, in discrete time steps $k\tau$, under an effective Hamiltonian matrix $f(\mathbf{H}) = -(\hbar/\tau) \cos^{-1} \mathbf{H}_s$, allowing standard time-dependent methods of analysis to be used in determining reaction probabilities.[49,52] The effective Hamiltonian matrix differs from $\mathbf{H}$ in a nonlinear fashion, so the "time" $k\tau$ is not physically meaningful. Indeed, τ is arbitrary and cancels in any formulas for observables. (This approach is also closely related to the "time-independent" wave packet approaches of Kouri and co-workers[53,54] and can be viewed as a generalization to reactive scattering of approaches developed by Chen and Guo.[55]) However, the magnitude of $\mathbf{q}^k$

is in fact a good approximation to the magnitude of the real part of an ordinary wave packet (evolving under $\mathbf{H}$ and starting from the same initial condition) at a physically meaninful time t_{phys} given by $t_{phys} \approx ka_s\hbar/(1 - E_s^2)^{1/2}$, where E_s is the mean scaled energy of the wave packet.[27] This approximation, based on the linearization of $f(\mathbf{H})$ about E_s is usually quite accurate owing to the fact that, with typical initial conditions, the wave packet's energy is concentrated in a narrow range in comparison with the full energy range.

The initial conditions for our propagations are given by the discrete analogs of $q^0 = \text{Re}\psi$,

$$\psi(R, r, \cos \gamma) = \sqrt{\frac{1}{\sqrt{\pi}\omega}} \exp\left(\frac{-(R - R_0)^2}{2\omega^2}\right) \times$$
$$\exp(-ik_0(R - R_0)) \chi_0(r)\bar{P}_0(\cos \gamma)|\alpha\rangle \quad (7)$$

which describes an incoming Gaussian wave packet in R with mean momentum $-\hbar k_0$, centered at $R = R_0$, and associated full width at half maximum of $2\omega \ln 2$. H$_2$ is initially in its ground vibration (χ_0) and rotation ($\bar{P}_0$) state, and the reactants are initially approaching on electronic state $|\alpha\rangle$. The recursion eq 6 requires $\mathbf{q}^0$ and $\mathbf{q}^1$ to be initiated. $\mathbf{q}^1$, if the initial condition is complex as it is in the present case, is evaluated according to $\mathbf{q}^1 = \mathbf{H}_s\cdot\mathbf{q}^0 - (1 - \mathbf{H}_s^2)^{1/2}\cdot\mathbf{p}^0$, where $\mathbf{p}^0$ is the imaginary part of the initial condition.[49] The action of the square root operator is itself accomplished with a Chebyshev expansion.[27]

Each iteration step eq 6 requires an evaluation of $\mathbf{H}$ on a real vector. Fast sine Fourier transforms are used to evaluate the relevant kinetic energy terms associated with R and r. The wave packet is kept in the Legendre basis above, which is convenient for evaluation of the relevant centrifugal term associated with $\mathbf{j}^2$ in eq 2. However, the potential terms are evaluated by transformation to a Gauss−Legendre quadrature grid associated with $\cos \gamma$, multiplication by the relevant potential terms on a full grid, and back transformation to the Legendre basis. This approach eliminates storage of large potential matrices. The calculations converge most favorably if the spectral range of the Hamiltonian is kept as small as possible without significantly altering accuracy. This is accomplished by introducing a cutoff energy V_{cut}, which is applied to all components of the diabatic electronic Hamiltonian as well as the centrifugal energy term.[27]

We estimate total reaction probabilities with a flux approach,[52] based on calculating the reactive flux on some surface separating reactants from products. In our case we define such a surface by $r = r^{\ddagger}$. (We should note that in the particular cases of the DIM propagation associated with α = Σ, as well as adiabatic 1A′ DIM propagation, there are much stronger long-range interactions relative to the DK surface, which lead to the underlying Σ or 1A′ potentials still showing some variation even at R_0 = 9.5 a_0. The determination of the total reaction probabilities also requires knowledge of the asymptotic distribution of momenta or energies in the initial wave packet. Because of the potential variation, the analytical form consistent with an incoming Gaussian has some error in it, particularly at low and high energy. We compensate for this by carrying out a back propagation on an effective one-dimensional potential to determine a more correct asymptotic distribution, as discussed in ref 28.

Typical grid and basis set details are given in Table 1. We carry out propagations to typically 20000−30000 iterations of eq 6. A typical coupled electronic state calculation, with the parameters in Table 1, requires ≈2.3 days of computational time on an IBM RS/6000 workstation and requires ≈80 MB of

TABLE 1. Typical Grid/Basis Set and Initial Condition Details.

reactant scattering coordinate (R) range/a_0	0−14.5
number of grid points in R	209
diatomic coordinate (r) range/a_0	0.5−11.5
number of grid points in r	127
number of angular grid points	40 (using potential symmetry)
number of angular basis functions	40 ($j = 0, 2, ..., 78$)
potential and centrifugal cut-off V_{cut}/eV	12
absorption in R starts at R_a/a_0	10.5
absorption strength in R, c_R/a_0^{-2}	0.005
absorption in r starts at r_a/a_0	7.5
absorption strength in r c_r/a_0^{-2}	0.005
center of initial wave packet R_0/a_0	9.5
Gaussian width factor ω/a_0	0.4
initial translational kinetic energy/eV	0.15
flux analysis line r†/a_0	6.0

memory. The single surface calculations with the same parameters require just under a day of computational time.

D. Trajectory Surface Hopping and Vibrationally Adiabatic Coupled Channel Calculations. For comparison with the wave packet results, two more approximate dynamical calculations are carried out for the case corresponding to reactants being initially on the Π state, which has the most interesting electronic coupling effects.

The trajectory surface hopping (TSH) calculations were carried out using Tully's fewest switches approach[36] as described by Schatz et al.[34] This TSH method involves simultaneous integration of the nuclear coordinates according to the classical equations of motion and of the amplitudes for being on the two electronic states according to a time-dependent Schrödinger equation. The only departure from ref 34 is that with one exception we used a diabatic representation for the TSH calculations rather than an adiabatic representation. This means that the trajectories and coupled Schrödinger equation were integrated using the diabats, and the $H_{\Sigma,\Pi}$ coupling. Also, the direction perpendicular to the intersection surface (used in adjusting the momenta after a surface hop) was chosen to be the gradient of the difference potential ($H_{\Sigma,\Sigma} - H_{\Pi,\Pi}$) rather than the derivative coupling vector. The one exception that we considered was for the DIM surface, where we were also able to use the adiabatic representation of ref 34 with the derivative coupling vectors from the DIM function. We used this calculation to determine the dependence of the results on which representation was used. We found that while both representations give roughly similar results, the diabatic representation results were much more accurate. For example, at 0.2 eV collision energy, the TSH adiabatic representation probability is 0.08, while the corresponding TSH diabatic representation probability is 0.20, and the (DIM, initial Π state) quantum wave packet result is 0.22. Note that because of the conversion between adiabatic and diabatic representations was done approximately, as discussed in section IIB, even the quantum results for the two representations should be different. Although we have not done wave packet calculations in the adiabatic representation (this would be quite difficult), we have assessed the internal consistency of the two representations by determining the derivative couplings that are based on the diabatic representation defined above for the DIM surface, and the results agree reasonably for geometries close to the conical intersection with those in the original adiabatic representation that was used to define the DIM diabats in the first place. As a result, we expect the quantum results will be fairly close for the two representations. In contrast to this, the TSH method, being approximate, should give different results in different representations, even if they are rigorously equivalent in their quantum dynamics. In the present application it turns out that

the Π state dynamics is closer to being diabatic than adiabatic (this is discussed in detail later), so TSH in the diabatic representation is less sensitive to the accuracy of the hopping algorithm than in the adiabatic representation. In fact, the TSH probability in the adiabatic representation is zero in the absence of hopping, so all of the reaction probability of 0.08 comes from the hopping algorithm, whereas in the diabatic representation the probability at 0.2 eV is already 0.11 in the absence of hopping, which means that hopping changes the probability from 0.11 to 0.22. Thus we see that hopping is of lesser importance in the diabatic representation than in the adiabatic representation. Since the diabatic representation results are more accurate, we restrict the TSH results presented later to those based on the diabatic representation.

In the TSH calculations, we considered $J = 0$ and integrated 100 trajectories per energy. The uncertainties associated with the TSH probabilities are estimated to be within ±5%. These calculations are quite time consuming for either the DK or DIM surfaces, requiring about a day of workstation time per energy. This is due to the DK and DIM surfaces being complicated functions that must be evaluated 10^4-10^5 times per trajectory, the small time steps needed to integrate the time-dependent Schrödinger equation accurately, and the fact that the trajectories can involve collision complexes. (Note the time-dependent Schrödinger equation referred to here is *not* the more rigorous one used in our wave packet calculations, but the one arising from the TSH model.) It would seem that the accurate quantum wave packet approach (which also generates information about all relevant energies at once) is more efficient! However, the effort needed to generate cross sections or rate constants with TSH is not much larger than the effort associated with the $J = 0$ TSH calculations, and the method scales much more favorably with dimensionality.

Approximate time-independent quantum results for the O+H$_2$ reaction were also obtained with a vibrationally adiabatic coupled channel method presented in more detail elsewhere.[35] In these studies the coupled channel equations were actually solved including all five electronic surfaces. The electronic states of the atom and the rotational states of the diatomic are included without any approximation to the vector coupling, or to the kinetic energy terms in the Hamiltonian. However, in order to keep the problem numerically tractable the diatomic vibration r is treated in an adiabatic fashion, and a limited rotational basis (most appropriate for relatively low collision energies) were employed. Also, the reactive flux is absorbed by using imaginary potentials in the interaction region before products have completely separated. The method was developed for the study of the effect of electronic Coriolis coupling on the reactive cross sections, but here results are presented for the Coriolis decoupled case for comparison with the wave packet calculations. Also, in these calculations we used the electronic Hamiltonian in eq 3 for the electrostatic coupling, rather than that in ref 35 that is based on a complex exponential basis. This leads to reaction probabilities that are consistent with the real-valued electronic functions employed in this paper. These scattering calculations involved using a basis of typically $j = 0$, 2, and 4 rotational states, along with all the appropriate projection states that are consistent with these values of j, for the five electronic states and a given value of J. For low J, this involves a small number of states (<20), so the computational time per energy is on the order of tens of seconds on a workstation. In contrast to the wave packet and TSH calculations, these calculations are trivial in terms of computational effort. The approximations invoked, however, limit their reliability to low collision energies.

Nonadiabatic Effects in O(^{1}D) + H$_2$ $\rightarrow$ OH + H

J. Phys. Chem. A, Vol. 103, No. 47, 1999 **9453**
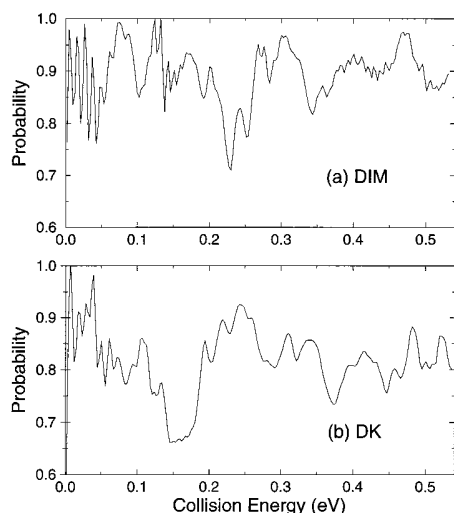
Figure 3. The total reaction probability for O(^{1}D) + H$_2$(X; $v = j = 0$) $\rightarrow$ OH(X) + H with total angular momentum $J = 0$ and assuming adiabatic dynamics on the ground 1A$'$ electronic state. (a) corresponds to the DIM 1A$'$ surface wave packet results, and (b) corresponds to the DK 1A$'$ surface wave packet results.

III. Results and Discussion

A. Adiabatic and Diabatic Single Surface Reaction Dynamics. The ground 1A$'$ adiabatic electronic state directly connects the reactants and products in reaction 1, and also correlates with the ground electronic state of H$_2$O. Adiabatic dynamics on this surface, is expected to be the most important contributor to the low energy reactive cross sections and moderate temperature rate constants. Figure 3 displays our quantum results for the total reaction probability associated with reaction 1, with the restrictions that the system have total angular momentum $J = 0$ and that H$_2$ initially be in its ground vibration-rotation state, $v = j = 0$. The total reaction probability reflects a sum over all energetically allowed OH(X$^2\Pi$) vibration–rotation states, v' and j'. (We do not investigate any details concerning the product distributions.) Both the 1A$'$ DIM surface result (Figure 3a) and the 1A$'$ DK surface result (Figure 3b) show that the total reaction probability is, on average, quite high. Both surfaces exhibit significant reaction probability at very low collision energies, consistent with the 1A$'$ surface having no barrier to reaction. While the DIM and DK reaction probabilities are roughly similar, the DIM surface is, on average, more reactive, than the DK surface. This reflects the fact that the DIM surface has stronger long range attraction than the ab initio DK surface. There is a lot of fine structure in Figure 3a and b, presumably because of the presence of numerous short-lived H$_2$O complexes and also due to the opening of various product v', j' channels. Similar behavior was seen in the adiabatic quantum dynamics of two other 1A$'$ potential energy surfaces.[26,27] Note also that the adiabatic 1A$'$ DK surface result was also previously obtained[28] in relation to a capture model study of total angular momentum effects. The convergence details of the resonance features in Figure 3 are similar to those of this earlier study.[28] In particular, the highest frequency features in Figure 3 at low collision energies do show some sensitivity to grid and propagation time details. However, if one averages over a small collision energy window of, say, 0.04 eV, we estimate that our reaction probabilities are converged to ±0.02 or 2%.

QCT studies[28,56] have also been performed for the 1A$'$ adiabatic dynamics. Using the surface of Ho et al.,[21] which is similar to the present DK surface, Aoiz[56] presented $J = 0$
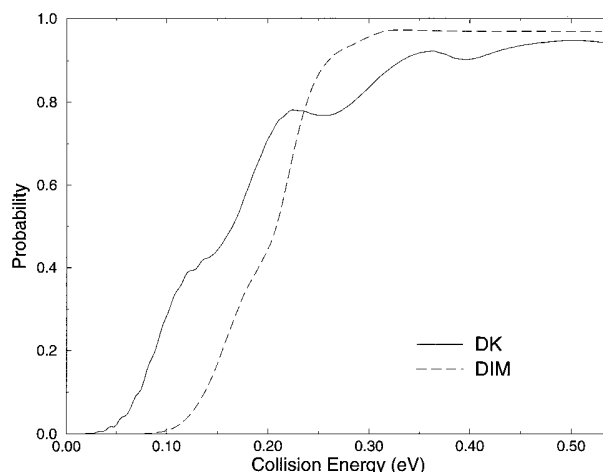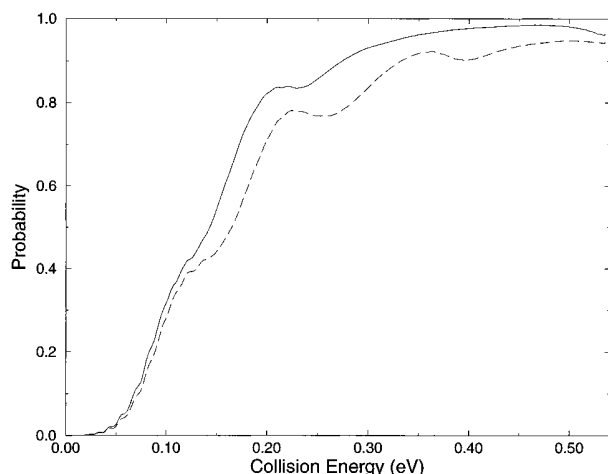

Figure 4. The total reaction probability for O(^{1}D) + H$_2$(X; $v = j = 0$) $\rightarrow$ OH(X) + H with $J = 0$, and assuming single surface dynamics on the Π diabatic state. The dashed curve corresponds to the DIM Π diabat wave packet results, and the solid curve corresponds to the DK Π diabat wave packet results.

reaction probabilities that were similar to but smoother than the corresponding quantum ones. These classical results were also generally upper bounds to the quantum ones. A $J = 0$ QCT study at one energy on the 1A$'$ DK surface also confirms this latter result.[28]

As indicated by Figure 1, adiabatic dynamics on the 2A$'$ surface cannot produce the desired OH(X$^2\Pi$) products, since it correlates with electronically excited OH(A$^2\Sigma$). Thus the reaction probability associated with reaction (1) is zero for this adiabatic surface. Similarly, in the diabatic representation discussed in sections I and II, the Σ diabat also correlates with OH(A) and therefore has no reactivity. The Π diabat, however, correlates with OH(X). Figure 4 shows the total reactivity associated with dynamics on the DIM (dashed curve) and DK (solid curve) Π diabats. These reaction probabilities are consistent with reaction being a direct and activated process on the Π diabat. The (collinear) barrier to reaction on the DIM Π diabat is ≈0.06 eV higher than the corresponding DK Π diabat (0.16 vs 0.10 eV), and this accounts for the DIM threshold for reaction being displaced to the right of the DK threshold in Figure 4. The DK Π diabat result in Figure 4 has more obvious step like structures than the DIM result. These structures are related to adiabatic thresholds associated with even excitations of the bending frequency (0.034 eV) at the collinear transition state. The associated DIM bending frequency (0.022 eV) is smaller, which brings the steps closer to one another so that they tend to a smoother structure.

As our final example of single surface dynamics, we consider the 1A$''$ surface, which also correlates with OH(X) products and has features similar to the Π diabat discussed above since for collinear geometries it is degenerate with this diabat. While the 1A$''$ and Π diabat surfaces coincide at collinear geometries, some differences occur at bent geometries. For example, the DK 1A$''$ surface exhibits a smaller bending frequency associated with motion away from the collinear saddle point. Figure 5 displays the DK 1A$''$ reaction probability (solid curve) and contrasts it with the DK Π diabat result (dashed curve), confirming that the 1A$''$ dynamics is similar to the Π diabat dynamics. However, as anticipated in the Introduction, the 1A$''$ reaction probability is slightly higher than the corresponding uncoupled Π diabat result. Recall that in order to construct the DIM diabatic model (section II) we actually assumed that Π diabat was the same as the 1A$''$ adiabat. The reasonably close

9454 *J. Phys. Chem. A, Vol. 103, No. 47, 1999*

Gray et al.

Figure 5. The solid curve corresponds to the total reaction probability for $O(^1D) + H_2(X; v = j = 0) \rightarrow OH(X) + H$ with $J = 0$, assuming adiabatic dynamics on the DK $1A''$ surface. The dashed curve is the corresponding Π diabat DK result for comparison.

correspondence of the curves in Figure 5 provides justification for this assumption.

B. Nonadiabatically Coupled Surfaces Reaction Dynamics.
In the asymptotic reactants limit, the Σ and Π diabats (sections I and II) are degenerate and one can determine all the relevant observable dynamics by considering initial conditions corresponding to any two linearly independent superpositions of Σ and Π. In particular, we consider an initial condition corresponding to reactants approaching initially on the pure Σ diabat, and another initial condition corresponding to reactants approaching on the pure Π diabat. What linear combinations of adiabatic ($1A'$ and $2A'$) states do these two particular pure diabatic initial conditions correspond to? One might naively anticipate simple symmetric and antisymmetric combinations of the $1A'$ and $2A'$ states but that is not the case. Consider the two-state mixing angle χ, given by $\tan(2\chi) = 2 H_{\Sigma,\Pi}/(H_{\Sigma,\Sigma} - H_{\Pi,\Pi})$. In a simple two-state picture one can relate the $1A'$ and $2A'$ states to the corresponding diabatic states according to[57]

$$|1A'\rangle = \cos \chi |\Sigma\rangle + \sin \chi |\Pi\rangle$$
$$|2A'\rangle = -\sin \chi |\Sigma\rangle + \cos \chi |\Pi\rangle \qquad (8)$$

As a function of R and $\cos \gamma$ with $r = 1.4$ a_0 one finds that for the R values of relevance to our initial conditions ($R \geq 9$ a_0), χ is relatively small for both the DK and DIM surfaces ($|\chi| \leq 0.1$ radians) which implies that the pure Σ diabat is, in fact, very close to a $1A'$ adiabatic state and, similarly, that the pure Π diabat is very close to a pure $2A'$ adiabatic state. This is convenient, since then the reaction probability for reaction 1 if we start in the $1A'$ ($2A'$) state is then essentially the same as the corresponding reaction probability if we start on the Σ (Π) state.

We first consider the case of $O(^1D) + H_2(X; v = j = 0)$ reactants initially approaching one another on the Σ diabat. In the absence of electronic coupling, as noted previously, this situation would lead to no products, i.e., zero reaction probability. Figure 6 displays as solid curves our calculated reaction probabilities. The nonadiabatic results on both the DIM (Figure 6a) and DK (Figure 6b) coupled surface systems indicate, in fact, a very high degree of reactivity occurs. These results, while not identical to the adiabatic $1A'$ results (indicated as dashed curves in Figure 6) are actually very similar to them, and exhibit many maxima and minima at approximately the same energies.
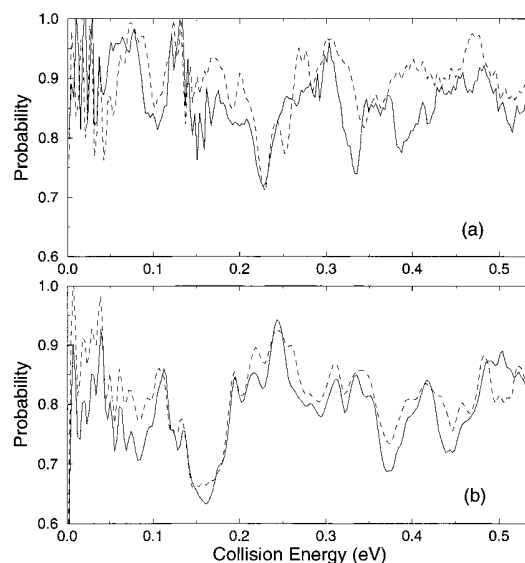
Figure 6. The solid curves correspond to the total reaction probability for $O(^1D) + H_2(X; v = j = 0)$ with $J = 0$, allowing for coupling of the Σ and Π diabats (or equivalently the $1A'$ and $2A'$ adiabatic states), with the initial reactant state being purely the Σ diabat, and the dashed curves correspond to the adiabatic results: (a) DIM surfaces, (b) DK surfaces.
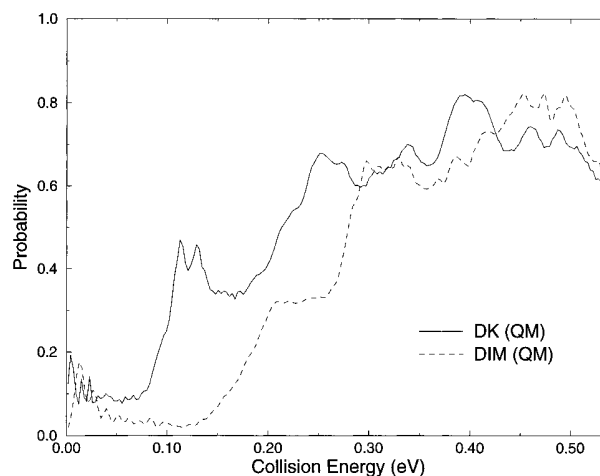
Figure 7. The total reaction probability for $O(^1D) + H_2(X; v = j = 0)$ with $J = 0$, allowing for coupling of the Σ and Π diabats, with the initial reactant state being purely the Π diabat: (a) DIM results, (b) DK results.

Electronic coupling in relation to the diabatic representation is very strong in this case, taking the pure Σ state into, effectively, a coherent superposition of Σ and Π states that corresponds to a good approximation of the $1A'$ adiabatic state. However, keeping the discussion of the above paragraph in mind, asymptotically the Σ and $1A'$ states are almost equivalent and so if we were to run our calculations in an adiabatic representation, starting from $1A'$, there would be very little coupling between the adiabatic states.

We next consider $O(^1D) + H_2(X; v = j = 0)$ initially approaching one another on the Π diabat. Recall that without electronic coupling the reaction probability was consistent with a direct, activated process and, at energies above the classical barrier was quite high (Figure 4). Figure 7 displays the resulting total reaction probabilities for the DIM (dashed curve) and DK (solid curve) surfaces, now allowing for coupling to the Σ surface to occur. There are at least two interesting features to note. First, the reaction probabilities at collision energies above

Nonadiabatic Effects in O(^{1}D) + H$_2$ → OH + H

J. Phys. Chem. A, Vol. 103, No. 47, 1999 **9455**

the collinear barrier can be significant, ranging between 0.4 and 0.8, which reflects a tendancy towards an uncoupled diabatic mechanism, similar in spirit to that seen in our pure Π diabat calculations of Figure 4. This represents the opposite of the near adiabatic limit noted above in relation to propagation of the Σ initial condition and can be interpreted as strong nonadiabatic coupling due to the conical intersection. However, the general magnitudes of the probabilities in Figure 7 can be 20% lower than the uncoupled results of Figure 4 at these higher collision energies and they also exhibit more structure, indicating that somewhat more complex dynamics is occuring. Note in particular that the steps in Figure 7 are more widely separated and more noticeable than in Figure 4. This suggests that the bottlenecks to reaction have moved from the saddle point region to shorter distances, such as near the conical intersection, where the bending frequency is higher.

The second interesting feature of the results in Figure 7 is at collision energies below the classical barrier to reaction. While these probabilities are small, on the order of magnitude of 0.1, they are non-zero even at very low energies close to the zero collision energy limit. Both the ab initio DK and the semiempirical DIM surfaces exhibit this behavior, although, interestingly, the ab initio surface shows a more significant low energy shoulder. These results are inconsistent with the barrier tunneling mechanism that is operative in the uncoupled Π diabat results (Figure 4), which leads to much smaller reaction probabilities. We experimented with the coupling term $H_{\Sigma,\Pi}$ and found that if it is exponentially damped for $R > 4.5\ a_0$ then the low collision energy probabilities become much smaller and behave just as in Figure 4, while the higher energy probabilities are not significantly affected and remain similar to those in Figure 7. Thus we have an interesting mechanism wherein the necessity of tunneling through the Π barrier at close range is avoided by Π to Σ transitions at longer range. Once amplitude grows on the Σ state at these larger distances it behaves more like the Σ, propagation results discussed in the above paragraph, i.e., it behaves more like the 1A′ adiabatic results, which exhibit nonzero reaction probabilities even at very low collision energies. (Notice also some fine resonance features that are apparent in Figure 7 at the low collision energies. These are similar to the resonance features in 1A′ and Σ propagations presented in Figure 6.)

Figure 8 further solidifies the points noted above in relation to the DK surface. The solid curve corresponds to the initial Π state propagation result of Figure 7 that includes electronic coupling. The dashed curve is the corresponding adiabatic 1A″ DK surface propagation result, which in turn is similar to the uncoupled Π diabat result (see Figure 5). Filled circles correspond to our TSH results consistent with the Π state propagation (which should be compared to the solid curve quantum result), and the open circles correspond to ordinary quasiclassical trajectory results on the 1A″ surface (which should be compared to the dashed curve quantum result). The dotted line with open diamonds corresponds to the vibrationally adiabatic scattering method of Drukker and Schatz,[35] which also should be compared with the solid curve quantum result. The TSH and 1A″ trajectory results are in reasonably good qualitative agreement with the corresponding quantum results. In particular, note that the TSH calculations (filled circles) do predict a finite reaction probability for the coupled diabats at very low energies, and this contrasts with the trajectory results for the 1A″ surface (open circles) at these energies. An examination of the TSH trajectories indicates that the hops that are responsible for this take place at relatively long range (R >
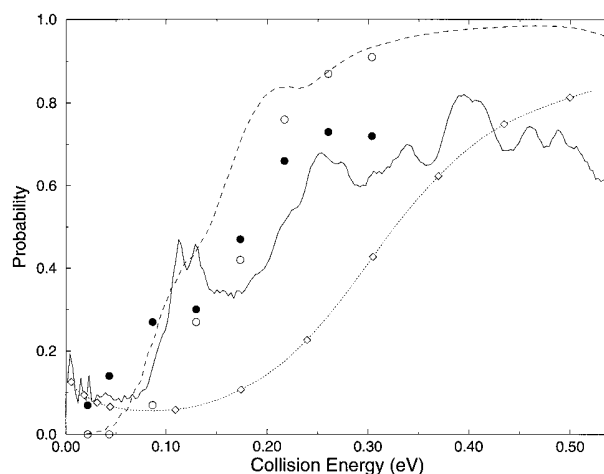

Figure 8. Various total reaction probability results for the DK surfaces are compared. The solid curve represents the nonadiabatically coupled quantum results with the reactant state being a pure Π state. The dashed curve corresponds to Π state dynamics with no nonadiabatic coupling allowed. The filled circles are trajectory surface hopping results. The open circles are adiabatic quasiclassical trajectory results for the 1A″ surface. The dotted line with open diamonds corresponds to the vibrationally adiabatic scattering approximation. See text for further details.

4 a_0). At higher energy, the 1A″ reaction probability rises up above the Π probability. Since the Π diabat is very similar to the 1A″ adiabat, some of the difference between reaction probabilities at high energy is due to trajectories which start out on the Π diabat, then transfer to the Σ diabat after surmounting the barrier, and then get reflected from the repulsive Σ potential for linear geometry. Finally we note that the vibrationally adiabatic quantum scattering approach[35] yields behavior qualitatively similar to the Π state propagation (solid curve), including the presence of a noticeable shoulder at low collision energies. The reaction probabilities for this approach show much less structure than the Π wave packet propagation results, and in the middle collision energy region, are somewhat lower than the Π results. The adiabatic treatment of r and the use of optical potentials that absorb amplitude in the well region are partly responsible for these deviations. Also, the rotational basis used in these calculations, while adequate for the low collision energy region, was really too small to describe bending threshold effects accurately. While for brevity we do not display the results, a very similar figure to Figure 8 was determined with the DIM surfaces.

We close this section on the coupled diabatic state dynamics by examining the O,H$_2$ angle γ averaged nuclear density contributions,

$$\rho_\alpha^k(R, r) = \sum_j |C_{j,a}^k(R, r)|^2 \qquad (9)$$

as the wave packets evolve, where α labels the diabatic electronic state and $C_{j,\alpha}^k(R, r)$ are the coefficients of the real wave packet of section II at iteration number k. Inspection of $\rho_\alpha^k(R, r)$ yields qualitative insights into the mechanism. Figure 9 displays ρ_α^k consistent with physical times $t_{phys} = 0, 75, 150$ and 225 fs for the DIM surfaces case with the initial wave packet on the Σ diabat. (Similar results were obtained with the DK surface.) This corresponds to actual iteration numbers $k = 0$, ≈ 2600, ≈ 5200 and ≈ 7800. Note that we carry out our calculations to much longer times or iteration numbers, e.g., iteration numbers on the order of 20,000 ($t_{phy} \approx 580$ fs), in
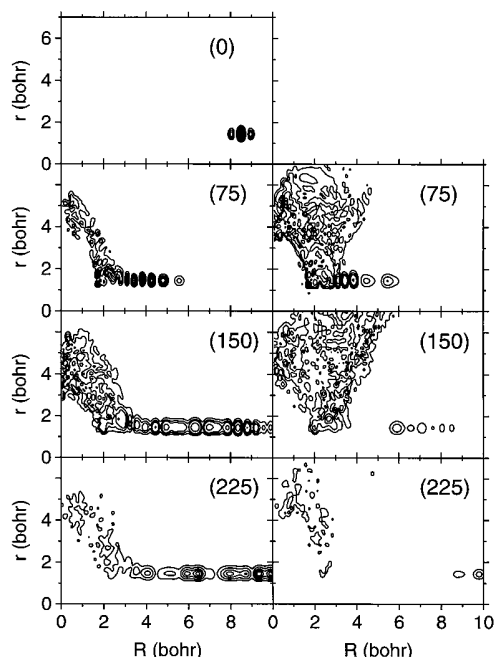
Figure 9. Contribution to the density from the real wave packet associated with the Σ and Π diabatic states for the case of the wave packet initially being on the Σ state. These results correspond to the DIM surface. The left column corresponds to the Σ state densities and the right column corresponds to the Π state densities. Approximate times t in femoseconds are indicated in brackets.

order to fine tune the reaction probability features. However most of the key dynamics is completed by much shorter times as is indicated by Figure 9. The left column of Figure 9 corresponds to the Σ state density and the right column of Figure 9 corresponds to the Π density. One sees the wave packet, initially localized on Σ approach the interaction region, spreading out also onto the Π state. Reaction can occur out of the Π state (right column) and that is most clearly indicated at $t_{phys} = 150$ fs in the figure with density streaming up to large r (and moderately large R). Notice also that significant density with R close to 0 au plays a role in the interaction region dynamics. This is the quantum equivalent of the insertion mechanism, which was also noted in an earlier 1A$'$ adiabatic surface quantum study.[27]

Figure 10 is similar to Figure 9 except it is the density for the case that we start on the DIM Π diabat. The dynamics is much simpler, with a direct mechanism on the Π diabat alone (right column) being evident. For example, at 75 fs one sees density streaming to the large r region consistent with products on the Π state. (The subsequent times 150 fs and 225 s are showing the nonreactive part of the wave packet going back down the reactant channel.) However, one also sees some nonadiabacity at 75 fs: the Σ state showing significant density has grown in the interaction region. One also sees some of this density tending to much smaller R values than the Π state density.

C. Rate Constant Estimates. In this subsection we make some approximate estimates of the effect of the nonadiabatic features noted above on the thermal rate constant for reaction 1 using the ab initio DK surface results. A completely rigorous calculation of the rate constant requires much more information than we have. For example, we would need to know the reaction probabilities for a number of total angular momenta $J > 0$, and we would also need to know these reaction probabilities for thermally populated initial vibration-rotation states of H$_2$, v,j.
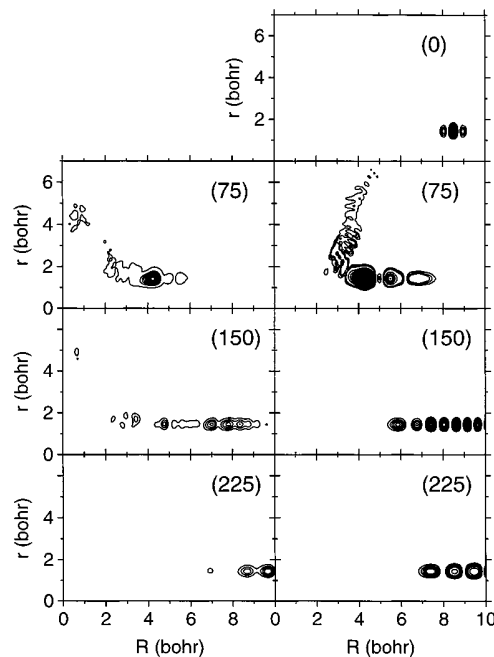
Figure 10. Density contribution associated with the Σ (left column) and Π (right column) diabatic states for the case of the wave packet initially being on the Π surface. Other details as those in Figure 9.

(More direct quantum approaches to obtaining $k(T)$ are also possible and can involve less work than calculating all the individual state-to-state information.[58]) The rigorous calculation of $k(T)$ for reaction (1) is clearly a formidable task. We have at our disposal here only J = 0 reaction probabilities out of H$_2$ in its ground vibration–rotation state, $v = j = 0$. We must make two approximations. First, we assume that the reaction probabilities (as a function of collision energy) are independent of v, j and equal to the $v = j = 0$ ones. As a consequence of this approximation, in what follows no thermal averages over v and j occur and it is always assumed that reaction probabilities or cross sections are those from $v = j = 0$. Second, we estimate the required J > 0 reaction probabilities from our $J = 0$ ones by employing either capture model ideas as previously invoked in a study of the 1A$'$ surface,[28] or J-shifting ideas.[46]

An earlier, more detailed study[28] of the J-dependence of the reaction probabilites on the 1A$'$ surface showed that J (or $J -$ shifting based on $J = 0$ reaction probabilities can lead to errors in the rate constant on the order of 15−20%. The assumption that cross sections are independent of the initial v, j state of H$_2$ and equal to the $v = j = 0$ ones is probably good for the 1A$'$ dynamics because, over the temperature range of interest (300−1000 K), $v = 0$ is the dominant contribution to the rate constant and it has also been shown that there is relatively little j dependence in the reaction probabilities.[21,26] The excited state (2A$'$ or Π and 1A$''$) dynamics is more sensitive to initial j,[33] and it is difficult to quantitfy the associated uncertainties introduced. However, the excited state contributions are in general relatively small and we expect these uncertainties to not be severe, i.e., less than the uncertainties introduced by J-shifting.

The rate constant for reaction 1 can be written as

$$k(T) = k_\Sigma(T) + k_\Pi(T) + k_{1A''}(T) \qquad (10)$$

where $k_\alpha(T)$ represents the contribution from initial electronic state $\alpha = \Sigma$, Π, or 1A$''$. In turn we can write each $k_\alpha(T)$ as an appropriate Boltzmann average of the corresponding reactive

Nonadiabatic Effects in O(^{1}D) + H$_2$ → OH + H

J. Phys. Chem. A, Vol. 103, No. 47, 1999 **9457**

cross section form state α, σ_α,

$$k_\alpha(T) = \frac{1}{5}\sqrt{\frac{8}{\pi\mu(k_B T)^3}}\int_0^\infty E_{col}\sigma_\alpha(E_{col})\exp(-E_{col}/k_B T)dE_{col} \tag{11}$$

where we have included the electronic degeneracy factor of 1/5 appropriate to reaction 1 in the prefactor. (An alternative would be to include the electronic degeneracy in the definition of σ_α. However, we are following the convention previously employed.[28,33]) The cross sections that enter into eq. 11 may be written in two ways. One way is

$$\sigma_\alpha(E_{col}) = \frac{\pi}{k_{col}^2}\sum_{J=0}^\infty (2J+1)P_\alpha^J(E_{col}) \tag{12}$$

where $k_{col} = \sqrt{2\mu E_{col}}/\hbar$. *J*-shifting approximations[46] can then be employed to approximate reaction probability P_α^J. Such approximations are most appropriate to direct reactions with barriers. In the case of a collinear transition state, the simplest *J*-shifting approximation is that the reaction probability $P_\alpha^J(E_{col}) = P_\alpha^{J=0}(\epsilon = E_{col} - J(J+1)B)$, where B is the rotational constant associated with the linear transition state ($B \approx 2$ cm^{-1} for the 1A″ state).

The second relevant form for σ_α is a sum over orbital angular momenta associated with the O,H$_2$ motion ℓ,[28]

$$\sigma_\alpha(E_{col}) = \frac{\pi}{k_{col}^2}\sum_{\ell=0}^\infty (2\ell+1)P_\alpha^\ell(E_{col}) \tag{13}$$

The ℓ-shifting approximation,[28] which is most appropriate when reaction is occurs via a capture process without any significant (bare) potential barrier, can then be invoked. This approximation is a quantum generalization of the classical capture or optical model that assumes the reaction probability is unity if a centrifugal barrier height is exceeded and zero otherwise. A simple ℓ-shifting approximation is $P_\alpha^\ell(E_{col}) \approx P_\alpha^{\ell=0}(\epsilon = E_{col} - V_\ell^*)$. Here, V_ℓ^* represents the centrifugal barrier height of an appropriate effective potential along R that includes the centrifugal term $\ell(\ell+1)/2\mu R^2$. (See ref 28 for more details.) Note that in the present case, with $j = 0$ initial state for H$_2$, $\ell = 0$ corresponds to $J = 0$ and so, as with the *J*-shifting approximation, only $J = 0$ information is needed.

In our calculations we have estimated the relevant cross sections and then rate constants for the DK surfaces using the formulae above. We employed the $J = 0$ reaction probabilities for the coupled electronic state Σ and Π initial states, as well as the $J = 0$ adiabatic reaction probabilities for the 1A″ state. It is clear that the *J*-shifting model outlined above is appropriate to the case α = 1A″ which, as discussed in the text, is an adiabatic reaction with a collinear transition state and direct dynamics. It is also reasonably clear that the ℓ-shifting approximation is appropriate to estimate the Σ state cross sections, since we showed in the previous subsection that the Σ dynamics was very similar to the insertion and capture dominated 1A′ dynamics. The relevant centrifugal barriers were determined just as in ref 28, employing the 1A′ adiabatic potential. (The Σ diabatic potential also leads to very similar results.) Which model is most appropriate to the Π propagation results is less clear since the low collision energy region is dominated by the long-range coupling mechanism (which would suggest an ℓ-shifting approximation based on the 1A′ adiabatic potential, would also be appropriate), and the higher collision energies

are dominated by a more direct diabatic mechanism that would suggest that the *J*-shifting approximation, based on the transition state for the Π diabat (which is the same as the 1A″ transition state) would be most appropriate. We discuss two results, a relatively low temperature ($T = 300$ K) for which the ℓ-shifting model was used for the Π rate constant estimate, and a high temperature result ($T = 1000$ K) for which the *J*-shifting approximation was used for σ_Π.

At $T = 300$ K we find, on the basis of the approximations above, that $k(T) = 1.0 \times 10^{-10}$ cm^3 s^{-1}. The experimental range is $1.0-1.4 \times 10^{-10}$ cm^3 s^{-1}.[21] The most significant contribution to this rate constant comes from k_Σ, which contributes 86% to the total. However, 13% of $k(T)$ is due to k_Π and the long range mechanism discussed in the previous subsection, and 1% is due to $k_{1A″}$. If *J*-shifting (instead of ℓ-shifting) were used to estimate k_Π, $k(T)$ would be lowered by 8% to 0.90×10^{-10} cm^3 s^{-1}, and the contribution to this from k_Π would be 7%, which is still a reasonable contribution. It is also of interest to contrast our $T = 300$ K estimate of the rate constant including nonadiabatic effects, 1.0×10^{-10} cm^3 s^{-1}, with the result based on purely adiabatic dynamics on the 1A′ surface, which we calculate to be 0.9×10^{-10} cm^3 s^{-1}. The purely adiabatic result is thus 10% lower than the nonadiabatic result. (The 1A′ adiabatic reaction probability, at low energies, includes some aspects of both the Σ and Π reaction probabilities, and so the purely adiabatic 1A′ result is a little higher and closer to the nonadiabatic result than might be expected.) At the higher temperature of $T = 1000$ K we find $k(T) = 1.5 \times 10^{-10}$ cm^3 s^{-1}, with ≈ 13% contributions from each of k_Π and $k_{1A″}$. Effects due to nonadiabatic dynamics are clearly largest here, with the purely adiabatic 1A′ estimate being just 1.2×10^{-10} cm^3 s, i.e., 20% lower.

IV. Concluding Remarks

A variety of calculations were carried out in order to assess the role of electronic nonadiabacity in the reaction of O(^{1}D) with H$_2$. We focused mostly on the coupled nuclear/electronic dynamics associated with two key electronic states. These states are the 1A′ and 2A′ adiabatic electronic states or, equivalently, certain Σ-like and Π(A′)-like diabatic electronic states. A conical intersection occurs between these states at collinear OHH geometries, and previous more approximate TSH studies,[34] and vibrationally adiabatic coupled channel studies,[35] have pointed to the possibility of interesting nonadiabatic effects.

Most of our calculations were quantum wave packet calculations based on the real wave packet methodology.[49,52] Our largest calculations corresponded to total angular momentum $J = 0$ wave packet propagations, including all three internal nuclear coordinates and the two electronic states within a diabatic representation. Several single surface wave packet propagations, and some TSH and vibrationally adiabatic coupled channel calculations were also carried out for comparison. We studied two different systems of coupled potential surfaces, a semiempirical DIM system due to Kuntz, Niefer, and Sloan,[30,31] and a recent ab initio system due to Dobbyn and Knowles.[44,45]

We confirmed that nonadiabacity is not an important issue if one starts effectively on the 1A′ potential energy surface. This is the surface that correlates with the ground electronic state of water and the reaction dynamics involves insertion coupled with some brief dynamics that can be associated with short-lived water complexes. No barrier exists for reaction on this surface, and significant reaction probabilities are seen for all collision energies examined, including very low collision energies. The dynamics of a wave packet initiated on, effectively, the 2A′ electronic state is much more interesting. In terms of the Σ and

Π(A′) diabatic representation we employed, an initial 2A′ state correlates with the Π(A′) state, which has a simple barrier to reaction at collinear geometries. One might expect strong nonadiabatic coupling (due to the conical intersection noted above) such that in a diabatic representation the system would *remain* on the Π diabat throughout (i.e., very little "nondiabatic coupling"). We do see evidence of this, particularly at collision energies above the collinear barrier. However, at low collision energies a new mechanism for reaction emerges—electronic transitions at long range that allow amplitude to avoid having to tunnel through the Π barrier. This leads to small but noticeable reaction probabilities even as the collision energy approaches zero. The TSH and vibrationally adiabatic coupled channel calculations also exhibit this behavior, further solidifying our conclusions. It is also noteworthy that the TSH results for the Π initial state case agreed reasonably well with the wave packet results, as just the opposite behavior has been found in studies of other reactions.[42,43] One significant difference associated with the present work is that the TSH calculations have been done in a diabatic representation, rather than the usual adiabatic representation, and the uncoupled diabats provide a better zero order description of the Π state dynamics.

We made estimates of the thermal rate constant for reaction at two temperatures, 300 K and 1000 K. These calculations were rather approximate, owing in part to the necessity of using *J*-shifting[46] and ∠shifting[28] techniques to infer $J > 0$ reaction probabilities from $J = 0$ ones. We showed that at 300 K nonadiabatic effects, especially the low collision energy mechanism noted above, could contribute 10% or more to the rate constant. At 1000 K nonadiabatic effects, as well as the contribution from the adiabatic 1A″ surface, are much more important and the rate constant is 20% larger than the single surface result based on the 1A′ adiabatic surface.

In view of the uncertainties introduced in our estimates of the rate constants (see section IIID), it is possible we are overestimating the relative contribution of nonadiabatic and excited state dynamics to the rate constants. It is therefore important to carry out much more detailed studies. Future work includes making better $J > 0$ estimates of the reaction probabilities, as well as an examination of the effect of H_2 initial vibration—rotation state.[59] It should be possible, for example, to carry out helicity decoupled calculations in the spirit of ref 28. Theoretical estimates of the differential cross sections, and how they are influenced by nonadiabatic effects, would also be very welcome, owing to the interesting experimental data that is becoming available.[39] Finally, we note that there are many other reactions with electronic states that behave as those in Figure 1, so the present results provide significant motivation for studying the role of excited electronic states more generally.

References and Notes

(1) Davidson, J. A.; Sadowski, C. M.; Schift, H. I.; Streit, G. E.; Howard, C. J.; Jennings, D. A.; Schmeltekopf, A. L. *J. Chem. Phys.* **1976**, *64*, 57.

(2) DeMore, W. B.; Sander, S. P.; Golden, D. M.; Hampson, R. F.; Kurylo, M. J.; Howard, C. J.; Ravishankara, A. R.; Kolb, C. E.; Molina, M. Chemical kinetics and photochemical data for use in stratospheric modeling. JPL publication 94-26; Jet Propulsion Laboratory, Pasadena, 1994.

(3) Talukdar, R. K.; Ravishankara, A. R. *Chem. Phys. Lett.* **1996**, *253*, 177.

(4) Laurent, T.; Naik, P. D.; Volpp, H. R.; Wolfrum, J.; Arusi-Parpar, T.; Bar, I.; Rosenwaks, S. *Chem. Phys. Lett.* **1995**, *236*, 343.

(5) Matsumi, Y.; Tonokura, K.; Kawasaki, M.; Kim, H. L. *J. Phys. Chem.* **1992**, *96*, 10622.

(6) Tsukiyama, K.; Katz, B.; Bersohn, R. *J. Chem. Phys.* **1985**, *83*, 2889.

(7) Butler, J. E.; MacDonald, R. G.; Donaldson, D. J.; Sloan, J. J. *Chem. Phys. Lett.* **1983**, *95*, 183.

(8) Jursich, G. M.; Wiesenfeld, J. R. *Chem. Phys. Lett.* **1985**, *119*, 511.

(9) Butler, J. E.; Jursich, G. M.; Watson, I. A.; Wiesenfeld, J. R. *J. Chem. Phys.* **1986**, *84*, 5365.

(10) Hsu, Y. T.; Wang, J. H.; Liu, K. *J. Chem. Phys.* **1997**, *107*, 2351.

(11) Buss, R. J.; Casavecchia, P.; Hirooka, T.; Sibener, S. J.; Lee, Y. T. *Chem. Phys. Lett.* **1981**, *82*, 386.

(12) Che, D. C.; Liu, K. *J. Chem. Phys.* **1995**, *103*, 5164.

(13) Alexander, A. J.; Aoiz, F. J.; Brouard, M.; Burak, I.; Fujimura, Y.; Short, J.; Simons, J. P. *Chem. Phys. Lett.* **1996**, *262*, 589.

(14) Hsu, Y. T.; Liu, K. *J. Chem. Phys.* **1997**, *107*, 1664.

(15) Casavecchia, P. Private communication.

(16) Ahmed, M.; Peterka, D. S.; Suits, A. G. *Chem. Phys. Lett.* **1999**, *301*, 372.

(17) Sorbie, K. S.; Murrell, J. N. *Mol. Phys.* **1976**, *31*, 905.

(18) Howard, R. E.; McLean, A. D.; Lester, W. A., Jr. *J. Chem. Phys.* **1979**, *71*, 2492.

(19) Schinke, R.; Lester, W. A., Jr. *J. Chem. Phys.* **1980**, *72*, 3754.

(20) Murrell, J. N.; Carter, S. *J. Phys. Chem.* **1984**, *88*, 4887.

(21) Ho, T. S.; Hollebeek, T.; Rabitz, H.; Harding, L. B.; Schatz, G. C. *J. Chem. Phys.* **1996**, *105*, 10472.

(22) Dunne, L. J. *Chem. Phys. Lett.* **1989**, *158*, 535.

(23) Aker, P. M.; Sloan, J. J.; Wright, J. S. *Chem. Phys.* **1986**, *110*, 275.

(24) Fitzcharles, M. S.; Schatz, G. C. *J. Phys. Chem.* **1986**, *90*, 3634.

(25) Aoiz, F. J.; Brouard, M.; Enriquez, P. A. *J. Chem. Phys.* **1996**, *105*, 4964.

(26) Peng, T.; Zhang, D. H.; Zhang, J. Z. H.; Schinke, R. *Chem. Phys. Lett.* **1996**, *248*, 37.

(27) Balint-Kurti, G. G.; Gonzalez, A. I.; Goldfield, E. M.; Gray, S. K. *Faraday Discuss.* **1998**, *110*, 169.

(28) Gray, S. K.; Goldfield, E. M.; Schatz, G. C.; Balint-Kurti, G. G. *Phys. Chem. Chem. Phys.* **1999**, *1*, 1141.

(29) Whitlock, P. A.; Muckerman, J. T.; Fisher, E. R. *J. Chem. Phys.* **1982**, *76*, 4468.

(30) Kuntz, P. J.; Niefer, B. I.; Sloan, J. J. *J. Chem. Phys.* **1988**, *88*, 3629.

(31) Kuntz, P. J.; Niefer, B. I.; Sloan, J. J. *Chem. Phys.* **1991**, *151*, 77.

(32) Walch, S. P.; Harding, L. B. *J. Chem. Phys.* **1988**, *88*, 7653.

(33) Schatz, G. C.; Papaioannou, A.; Pederson, L. A.; Harding, L. B.; Hollebeek, T.; Ho, T. S.; Rabitz, H. *J. Chem. Phys.* **1997**, *107*, 2340.

(34) Schatz, G. C.; Pederson, L. A.; Kuntz, P. J. *Faraday Discuss.* **1997**, *108*, 357.

(35) Drukker, K.; Schatz, G. C. *J. Chem. Phys.* **1999**, *111*, 2451.

(36) Tully, J. C. *J. Chem. Phys.* **1990**, *93*, 161.

(37) Hammes-Schiffer, S.; Tully, J. C. *J. Chem. Phys.* **1994**, *101*, 4657.

(38) Alexander, A. J.; Blunt, D. A.; Brouard, M.; Simons, J. P.; Aoiz, F. J.; Banares, L.; Fujimura, Y.; Tsubouchi, M. *Faraday Discuss.* **1997**, *108*, 375.

(39) Alagia, M.; Balucani, N.; Cartechini, L.; Casavecchia, P.; van Kleef, E. H.; Volpi, G. G.; Kuntz, P. J.; Sloan, J. J. *J. Chem. Phys.* **1998**, *108*, 6698.

(40) Hsu, Y. T.; Liu, K.; Pederson, L. A.; Schatz, G. C. *J. Chem. Phys.* In press.

(41) Lee, S.-H.; Liu, K. *J. Chem. Phys.* **1999**, *0000*, 0000.

(42) Topaler, M. S.; Hack, M. D.; Allison, T. C.; Liu, Y. P.; Mielke, S. L.; Schwenke, D. W.; Truhlar, D. G. *J. Chem. Phys.* **1997**, *106*, 8699.

(43) Allison, T. C.; Mielke, S. L.; Schwenke, D. W.; Truhlar, D. G. *J. Chem. Soc. Faraday Trans.* **1997**, *93*, 825.

(44) Dobbyn, A. J.; Knowles, P. J. *Mol. Phys.* **1997**, *91*, 1107.

(45) Dobbyn, A. J.; Knowles, P. J. *Faraday Discuss.* **1998**, *110*, 247.

(46) Bowman, J. M. *J. Phys. Chem.* **1991**, *95*, 4960.

(47) Rebentrost, F.; Lester, W. A., Jr. *J. Chem. Phys.* **1975**, *63*, 3737.

(48) Dobbyn, A. J.; Connor, J. N. L.; Besley, N. A.; Schatz, G. C.; Knowles, P. J. *Phys. Chem. Chem. Phys.* **1999**, *1*, 957.

(49) Gray, S. K.; Balint-Kurti, G. G. *J. Chem. Phys.* **1998**, *108*, 950.

(50) Mandelshtam, V. A.; Taylor, H. S. *J. Chem. Phys.* **1995**, *102*, 7390.

(51) Mandelshtam, V. A.; Taylor, H. S. *J. Chem. Phys.* **1995**, *103*, 2903.

(52) Meijer, A. J. H. M.; Goldfield, E.; Gray, S. K.; Balint-Kurti, G. G. *Chem. Phys. Lett.* **1998**, *293*, 270.

(53) Huang, Y.; Kouri, D. J.; Hoffman, D. K. *J. Chem. Phys.* **1994**, *101*, 10493.

(54) Huang, Y.; Iyengar, S. S.; Kouri, D. J.; Hoffman, D. K. *J. Chem. Phys.* **1996**, *105*, 927.

(55) Chen, R.; Guo, H. *J. Chem. Phys.* **1996**, *105*, 3569.

(56) Aoiz, F. J. *Faraday Discuss.* **1998**, *110*, 245.

(57) Rebentrost, F. *Theoretical Chemistry: Advances and Perspectives*; Henderson, D., Ed.; Academic: New York, 1981; Vol. 6B, p 1.

(58) Miller, W. H. *Acc. Chem. Res.* **1993**, *26*, 174.

(59) Balint-Kurti, G. G.; Gray, S. K.; Schatz, G. C. To be submitted.